



Gadolinium-Coated Mesoporous Silica Nanoparticle for Magnetic Resonance Imaging

Zhongtao Li¹, Jing Guo¹, Mengmeng Zhang¹, Guohua Li^{2*} and Liguao Hao^{1,3*}

¹Department of Molecular Imaging, School of Medical Technology, Qiqihar Medical University, Qiqihar, China, ²Department of Radiology, The First Affiliated Hospital of Qiqihar Medical University, Qiqihar, China, ³Department of Molecular Imaging, The First Affiliated Hospital of Qiqihar Medical University, Qiqihar, China

Magnetic resonance molecular imaging can provide anatomic, functional and molecular information. However, because of the intrinsically low sensitivity of magnetic resonance imaging (MRI), high-performance MRI contrast agents are required to generate powerful image information for image diagnosis. Herein, we describe a novel T_1 contrast agent with magnetic-imaging properties facilitated by the gadolinium oxide (Gd_2O_3) doping of mesoporous silica nanoparticles (MSN). The size, morphology, composition, MRI relaxivity (r_1), surface area and pore size of these nanoparticles were evaluated following their conjugation with Gd_2O_3 to produce $Gd_2O_3@MSN$. This unique structure led to a significant enhancement in T_1 contrast with longitudinal relaxivity (r_1) as high as $51.85 \pm 1.38 \text{ mM}^{-1}\text{s}^{-1}$. $Gd_2O_3@MSN$ has a larger T_1 relaxivity than commercial gadolinium diethylene triamine pentaacetate (Gd-DTPA), likely due to the geometrical confinement effect of silica nanoparticles. These results suggest that we could successfully prepare a novel high-performance T_1 contrast agent, which may be a potential candidate for *in-vivo* MRI.

Keywords: gadolinium oxide, mesoporous silica nanoparticle, magnetic resonance imaging, cytotoxicity, contrast agent

1 INTRODUCTION

Magnetic resonance imaging (MRI) is non-invasive and produces high-resolution morphological and innate three-dimensional image resolution without the risk of radiation damage, making it a critical clinical diagnostic tool. MRI contrast agents are a specific substrate used in these technologies to help improve the contrast between normal and abnormal tissues. Gadolinium diethylene triamine pentaacetate (Gd-DTPA) remains the most common MRI contrast agent as it can enhance the brightness of the region of interest (ROI; positive contrast) (Shin et al., 2015; Ni et al., 2017; Shen et al., 2017). However, Gd-DTPA is a small-molecule contrast agent and suffers from relatively low sensitivity, specificity, and relaxivity, which limits its applications in more complex diagnostic settings (Fraum et al., 2017; Vikas et al., 2017). This implies that alternative contrast agents, specifically those commonly referred to as gadolinium-based T_1 contrast materials have begun to attract more attention.

In addition, nano-drug delivery systems (NDDS) are currently amongst the most evaluated drug delivery systems in the world. These NDDS combine a therapeutic payload with nano-sized carriers (such as liposomes, gold nanoparticles, polymeric micelles, and mesoporous silica) to reduce side effects and prolong circulation time (Mikada et al., 2017; Layek et al., 2020). Thus, the introduction of

OPEN ACCESS

Edited by:

Wansong Chen,
Central South University, China

Reviewed by:

Lin Liu,
Anyang Normal University, China
Tongtong Xuan,
Xiamen University, China

*Correspondence:

Liguao Hao
haoliguao@qmu.edu.cn
Guohua Li
liguohua@qmu.edu.cn

Specialty section:

This article was submitted to
Nanoscience,
a section of the journal
Frontiers in Chemistry

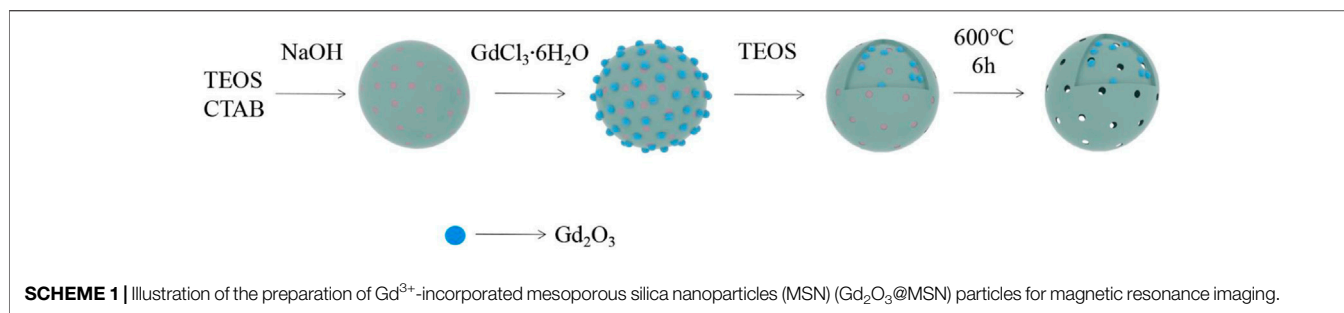
Received: 16 December 2021

Accepted: 24 January 2022

Published: 15 February 2022

Citation:

Li Z, Guo J, Zhang M, Li G and Hao L
(2022) Gadolinium-Coated
Mesoporous Silica Nanoparticle for
Magnetic Resonance Imaging.
Front. Chem. 10:837032.
doi: 10.3389/fchem.2022.837032



MRI contrast agents into an NDDS may both extend blood circulation time and improve MRI performance (because of the shortened longitudinal proton relaxation time of the surrounding water molecules for T_1 -type contrast agents) (Lin et al., 2004; Parvesh et al., 2012; Li et al., 2014; Hu et al., 2015; Deng et al., 2016; Wang and Sun, 2020). Of the common NDDS carriers mesoporous silica nanoparticles (MSNs) are widely used in the carriers for drug delivery and biosensing and are likely to be the most appropriate carrier for gadolinium owing to their high surface area, ease of preparation, good biocompatibility, and mesoporous structure (Lin et al., 2004; Taylor et al., 2008; Xia et al., 2019). Additionally, the overall structure is composed of silica and Si-OH groups. Si-O-Si frameworks are quite stable and silica degradation is relatively difficult under physiological conditions, which means that these particles are likely to facilitate good loading of Gd_2O_3 but inhibit the release of free Gd^{3+} reducing its toxic effects.

Herein, we report a novel synthesis system for producing Gd^{3+} -incorporated MSN (Gd_2O_3 @MSN), which are characterised by a mesoporous structure, higher surface area and high T_1 relaxivity. These nanoparticles (NPs) are easy to prepare and modify, present with low-cost, and possess desirable MRI contrast-enhancement properties, thus making them suitable for the creation of more specific, and possibly even targeted, contrast agents for molecular MRI and could help provide real-time feedback for treatment outcomes (Scheme 1), potentially enhancing the clinical utility of MRI.

2 MATERIALS AND METHODS

2.1 Materials

Hexadecyl trimethyl ammonium bromide (CTAB, 99%) was purchased from Coolaber Science & Technology. Tetraethoxysilane (TEOS, 99%) was purchased from Fuchen Chemical Reagents (Tianjin, China). 3-Aminopropyltriethoxysilane (99%) was purchased from Macklin Biochemical Co., Ltd. (Shanghai, China). Gadolinium (III) chloride hexahydrate ($\text{GdCl}_3 \cdot 6\text{H}_2\text{O}$, 99.9%) was purchased from Aladdin Biochemical Technology Co., Ltd. (Shanghai China).

2.2 Preparation of Gd_2O_3 @MSN

Briefly, NaOH (140 mg) and CTAB (500 mg) were dissolved in 220 ml of deionised water and stirred (300 rpm) at 80°C for 1 h.

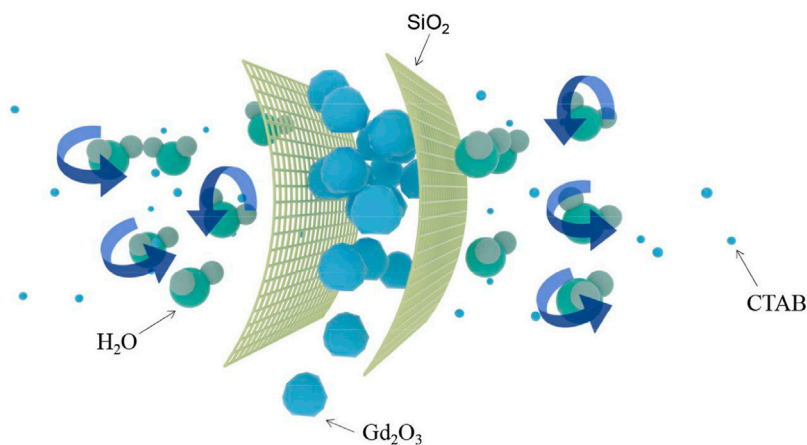
Next, we slowly added TEOS (1.8 ml) in a dropwise manner to this suspension while maintaining the stirring (250 rpm) of the recipient solution. This mixture was then stirred for another 2 h and then 20 ml of $\text{GdCl}_3 \cdot 6\text{H}_2\text{O}$ aqueous solution (5 mg/ml) was quickly added into the mixture. One hour later, an additional 0.7 ml of TEOS was added to these samples, left for an additional 2 h, centrifuged, washed with ethanol and deionised water, and then dried in an oven at 50°C for 24 h. The resulting Gd_2O_3 @MSN were collected and calcined at 600°C for 6 h to remove CTAB surfactants.

2.3 Characterizations

Gd_2O_3 @MSN (1 mg/ml) particle size and zeta potential was confirmed by dynamic light scattering (Malvern Zetasizer Nano ZS system, Malvern, Worcestershire, United Kingdom). We then performed transmission electron microscopy (TEM) (FEI Talos F200S, United States) to examine the surface morphology of the Gd_2O_3 @MSN particles. Their composition was evaluated by energy dispersive X-ray spectroscopy (EDS). Scanning transmission electron microscopy high-angle annular dark-field (STEM-HAADF) images and energy-dispersive X-ray (EDX) element mapping images were obtained using an FEI Talos F200S microscope at an accelerating voltage of 300 kV. The analysis of the N_2 adsorption isotherms was performed using Barrett-Joyner-Halenda (BJH) analysis (Micromeritics ASAP-2460, Norcross, GA, United States). The surface area, total pore volume, and average pore distribution curves for the MSNs were determined using the Brunauer-Emmett-Teller (BET) method. Fourier transform infrared refraction (FT-IR, RF-5301PC, Shimadzu, Japan) analyses of the Gd_2O_3 @MSN particles were performed in the range of 400 – $4,000\text{ cm}^{-1}$ or structural characterization.

2.4 T_1 Relaxivity and *in-vitro* Magnetic Resonance Imaging of as-prepared NPs

The Gd^{3+} concentration of the doped MSNs was proved using Inductively-coupled plasma mass spectrometry (ICP-MS, Agilent 720 ES, United States), and ICP-MS was also used to detect whether free Gd elements were dissociated from Gd_2O_3 @MSNs when immersed in phosphate-buffered saline (PBS) at different pH (7.4, 5.5 and 4.5) for 48 h. Next we evaluated the T_1 relaxivity of Gd_2O_3 @MSN and Gd-DTPA with different molar



SCHEME 2 | The removal of hexadecyl trimethyl ammonium bromide and the formation of Gd_2O_3 .

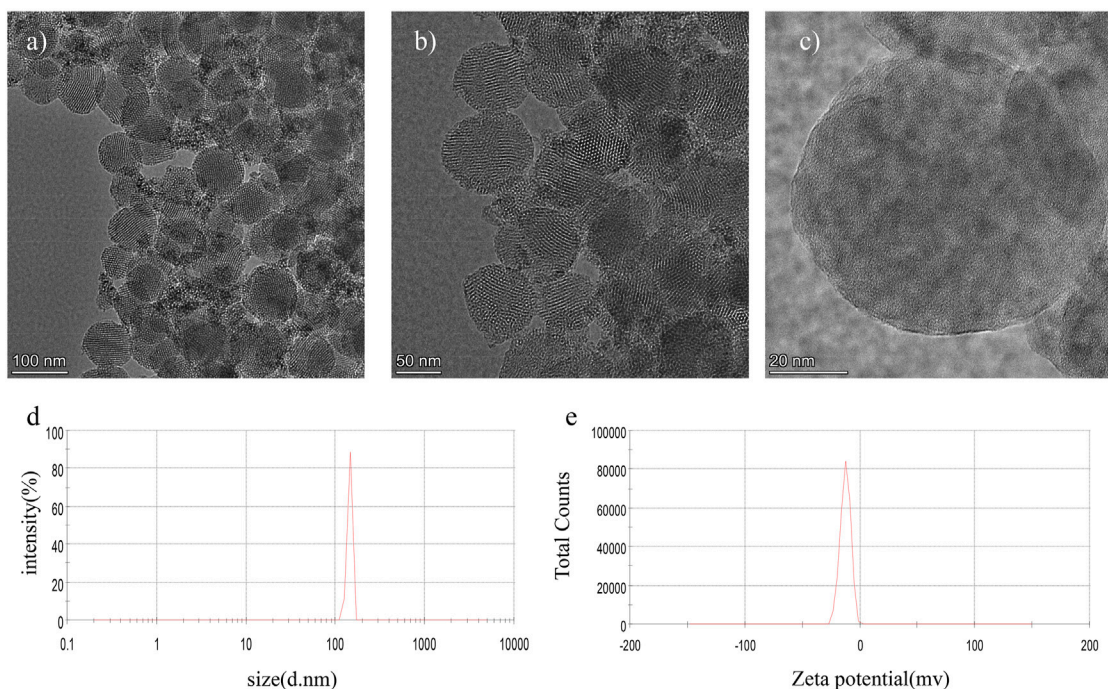


FIGURE 1 | Structural evaluation of Gd_2O_3 @mesoporous silica nanoparticles by **(A–C)** transmission electron microscopy; **(D)** dynamic light scattering; and **(E)** zeta potential evaluation.

concentrations of gadolinium when kept in 1% agarose solution using a 0.5 T NMI20 Analyst NMR system (Niumag Analytical Instrument Corporation, Sunzhou, China) (Repeat three times for each sample) set to apply the following parameters: SW: 100 kHz, TW: 3,000 ms, RFD: 0.08 ms, NS: 8, TE: 1 ms and NTI: 25 (in pure water, 37°C), and the T_1 graph was obtained using the inversion recovery (T_1 -TSE) sequence: TR/TI: 3,000/20 ms, TE: 20 ms, matrix: 256 × 192, layer thickness: 3 mm, FOV: 90 × 120 mm.

2.5 In-Vitro Evaluations

2.5.1 Cell Culture

The human pancreatic cancer cell line AsPC-1, PaCa-2 and 4T1 breast cancer line were purchased from the Shanghai Cell Bank of the Chinese Academy of Sciences and cultured in Roswell Park Memorial Institute 1,640 (RPMI 1640) medium containing 10% (v/v) foetal bovine serum (FBS) and 1% penicillin/streptomycin. The cell lines were cultured using regular cell culture conditions (37°C with 5% CO_2).

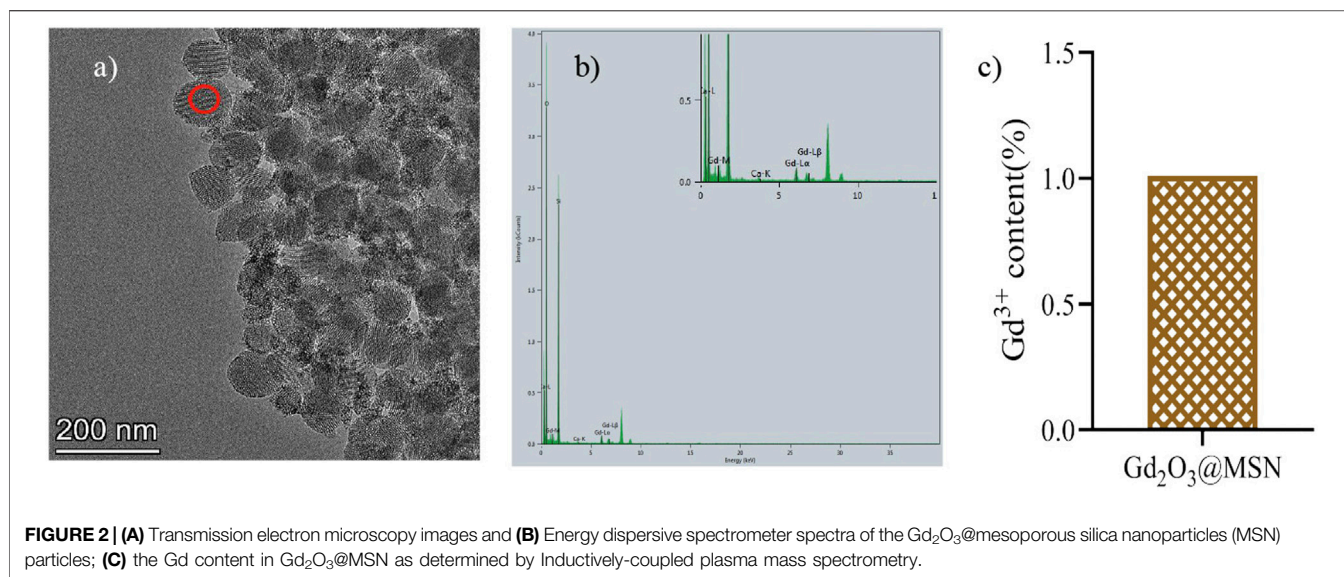


TABLE 1 | Results of energy dispersive X-ray spectroscopy analysis of the $Gd_2O_3@mesoporous\ silica$ nanoparticles particles.

Location	Si (atom.%)	O (atom.%)	Gd (atom.%)
Red circle	30.53	68.56	0.91

2.5.2 Cytotoxicity Assay

AsPC-1, PaCa-2 and 4T1 cells were separately plated in 96-well plates (5×10^3 cells/well) with 100 μ L of medium and incubated for 24 h before the culture medium was replaced with 100 μ L of RPMI 1640 supplemented with different concentrations of $Gd_2O_3@MSN$ (5, 25, 50, 100, 150 and 200 μ g/ml) and incubated for an additional 24 h. The drug-containing culture medium was then removed and replaced with 100 μ L of fresh medium and 10 μ L of CCK-8 and incubated for 2 h before measuring the absorbance at 490 nm using a plate reader (SAFIRE2, TECAN, Switzerland). Cell viability was then calculated using the following equation: Cell viability (%) = $(A_{treated} - A_{blank}) / (A_{control} - A_{blank}) \times 100\%$. where $A_{treated}$, $A_{control}$ and A_{blank} represent the absorbance of the treated, control and blank wells, respectively.

2.6 In-Vivo Evaluations

2.6.1 Experimental Animals

Male SPF-grade Sprague–Dawley (SD) rats (180 ± 10 g) were purchased from Liaoning Changsheng biotechnology Co., Ltd. (SXK2020-0001) and housed as prescribed. The animal experiments were approved by the Animal Ethics Committee of Qiqihar Medical University (No. QMU-AECC-2021-168).

2.6.2 In-Vivo Toxicity Studies

Ten healthy SD rats (180 ± 10 g) were randomly divided into two groups (five rats in each). The rats were then injected

with 100 mg/kg $Gd_2O_3@MSN$ or saline. After 7 days, all the rats were sacrificed and approximately 3 ml of blood was collected from each rat for blood chemistry evaluations immediately before being euthanised. Then, the major organs, namely the heart, liver, spleen, lung, and kidneys, were harvested from those rats for H&E staining and histopathological examination (Leica-DM4B digital microscope, Germany).

2.6.3 In-Vivo Magnetic Resonance Imaging Studies

These experiments were performed using a Philips (Achieva 3.0 T) MRI scanner with 8-channel carotid wall imaging special phased array coil. Male SD rats were selected for T_1 -weighted MRI from each group ($n = 3$) and injected with $Gd_2O_3@MSN$ or Gd-DTPA at 0.5 mg of Gd^{3+} per kg of body weight. The images were then produced using a T_1 sequence with the following parameters: TR/TE = 650/10 ms, thickness = 3 mm, 192×192 matrices, FOV = 130×130 mm and flip angle = 90° . The signal-to-noise ratio (SNR) for each image was then calculated by analysing each ROI (in each image). Contrast enhancement was defined as an increase in SNR after injection using the following equation:

$$\Delta SNR = (SNR_{post} - SNR_{pre}) / SNR_{pre}$$

All image data were transferred to a remote computer for analysis.

2.7 Statistical Analysis

Nanoparticle size was analysed using the Nano Measure 1.2 software, and SPSS 20.0 (SPSS Inc., Chicago, United States) was used for data management and statistical analysis (Student's t-test for unpaired data). The data are expressed as the mean \pm standard deviation. A p -value of <0.05 is considered statistically significant and the SNR values were determined using ImageJ.

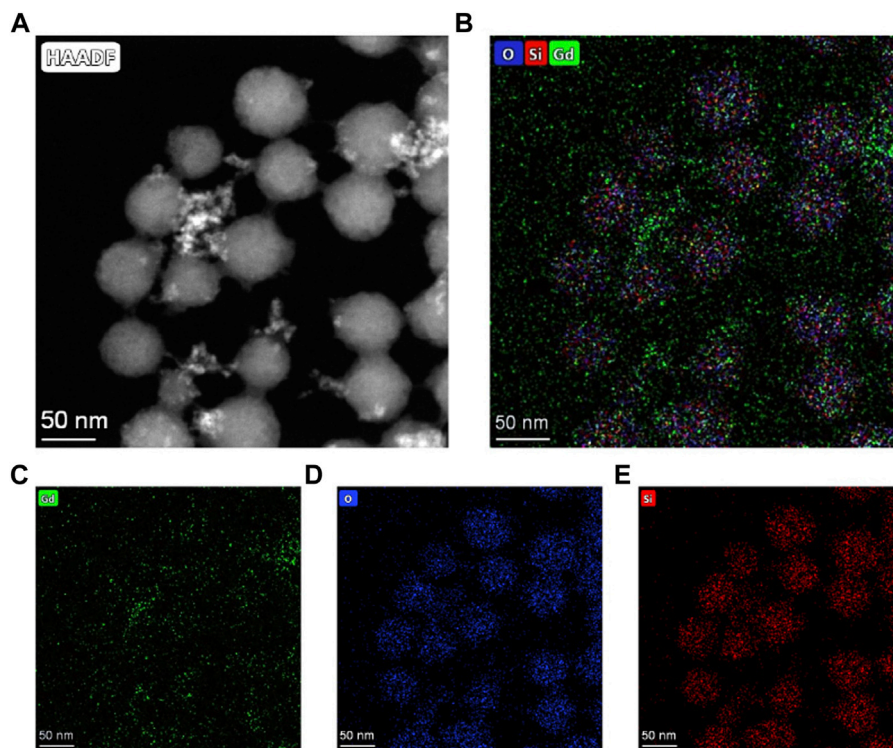


FIGURE 3 | (A) Scanning transmission electron microscopy high-angle annular dark-field images of $Gd_2O_3@MSN$ nanocomposites and (B–E) Elemental mapping images of $Gd_2O_3@MSN$ nanocomposites, confirming that Gd^{3+} elements were evenly distributed across MSN structure.

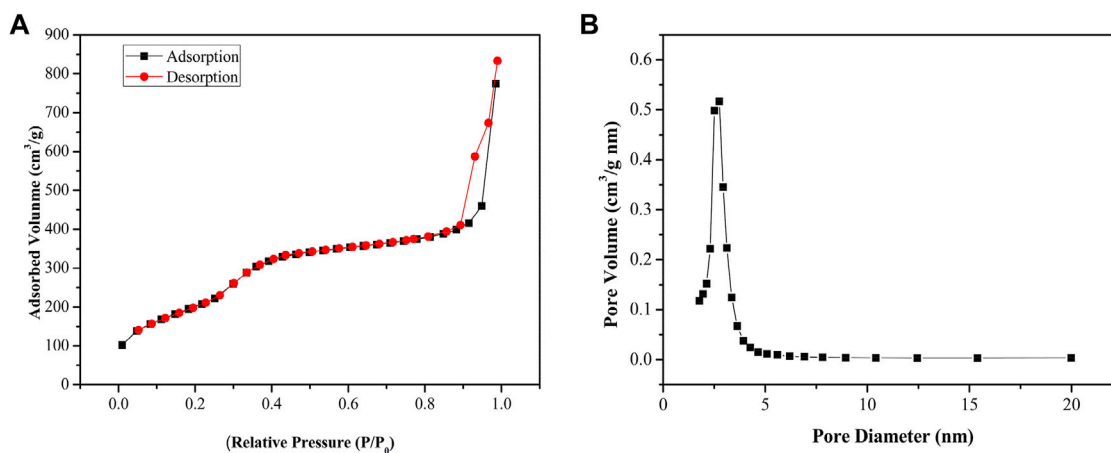


FIGURE 4 | (A) Nitrogen adsorption–desorption isotherms. (B) Pore size distribution curves, indicating an average pore size of about 3.49 nm for these $Gd_2O_3@$ mesoporous silica nanoparticles.

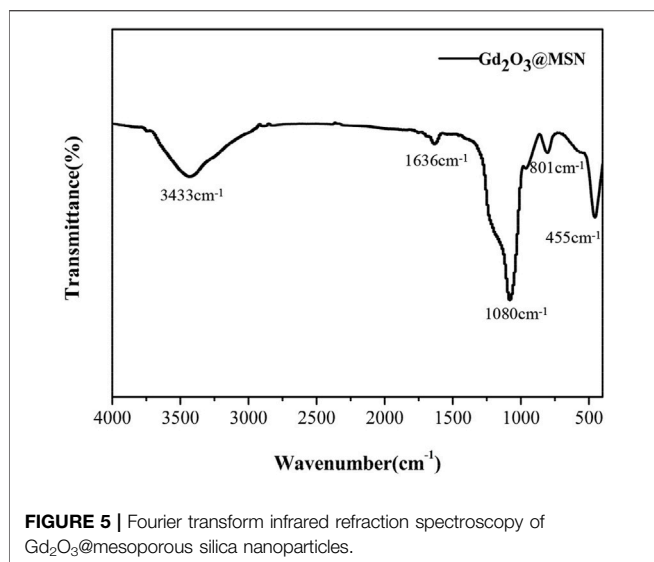
3 RESULTS AND DISCUSSION

3.1 Preparation and Characterization of $Gd_2O_3@MSN$

Our preparation used CTAB as the template and TEOS as the main silica source. First, solid silica nanospheres containing the CTAB template were prepared and then Gd^{3+} was converted to

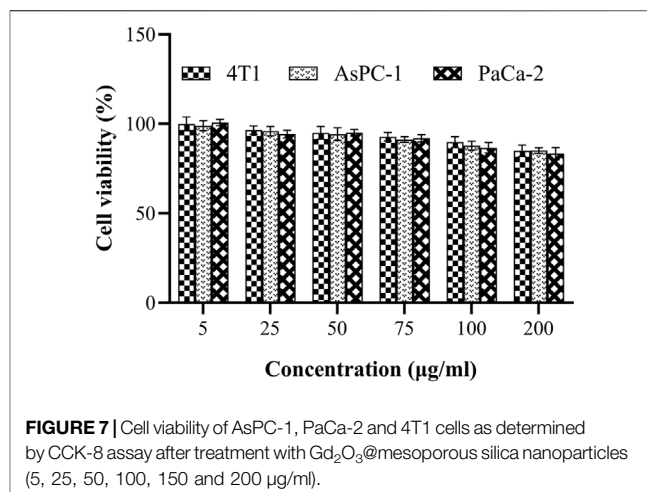
$Gd(OH)_3$ in alkaline solution ($pH = 9$), before being used to coat the surface of the SiO_2 nanospheres. Once the *mesoporous silica shell* successfully coated the solid core, the final product was calcined at $600^\circ C$ for 6 h to remove the CTAB template and dehydrate $Gd(OH)_3$ to Gd_2O_3 (Scheme 2).

Figure 1 described the structural characteristics of the prepared $Gd_2O_3@MSN$. TEM (Figures 1A–C) revealed that



these NPs were spherical or ellipsoid in shape and of uniform size and distribution, and the mean diameter of these NPs was determined to be 86.85 ± 10.44 nm. Dynamic light scattering (DLS) curves (**Figure 1D**) revealed that the average diameter of the NPs was 162.50 nm, suggesting that the DLS measured these NPs as slightly larger than the TEM, which might be the result of the rehydration of the NPs in the aqueous solution used for the DLS evaluation. As expected, the zeta potential of the MSN was negative (**Figure 1E**), whereas the moderate size of these particles should help avoid renal clearance and uptake to the reticuloendothelial system (RES) in the liver, which were both essential for increasing circulation time (Phillips et al., 2010; Koo et al., 2011; Shao et al., 2011; O'Connell et al., 2017; Jiang et al., 2019).

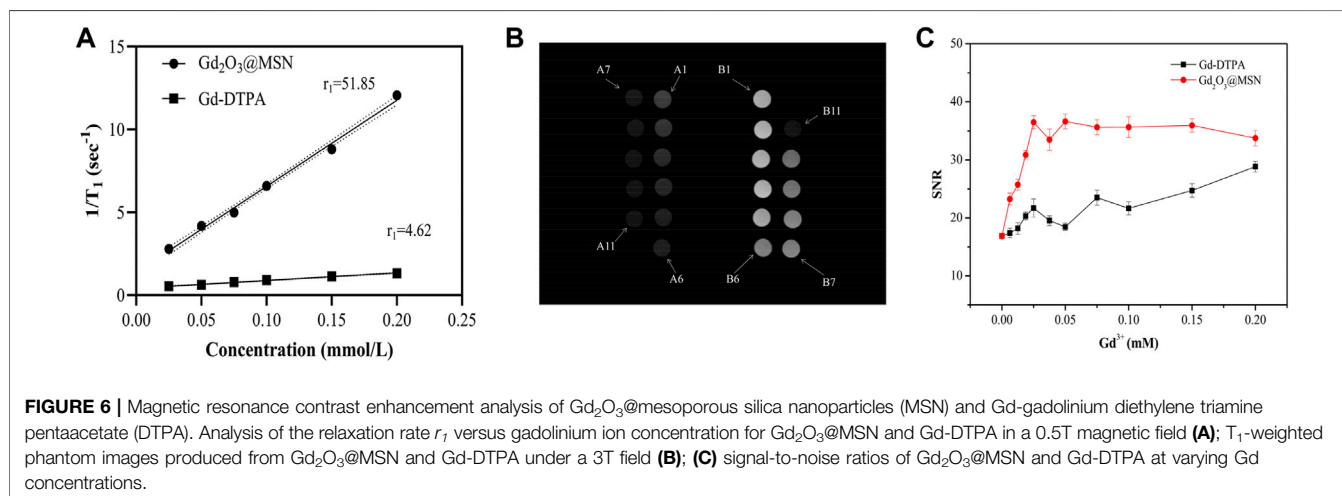
The EDS (**Figure 2B**) spectrum confirmed that the red circle appearing in **Figure 2A** indicates Gd-existence with an atomic fraction of 0.91% (atom.%) Gd (**Table 1**). ICP-MS (**Figure 2C**) determined the overall Gd concentration to be 1.01 (atom. %). We then investigated the structure of NPs in detail. STEM-

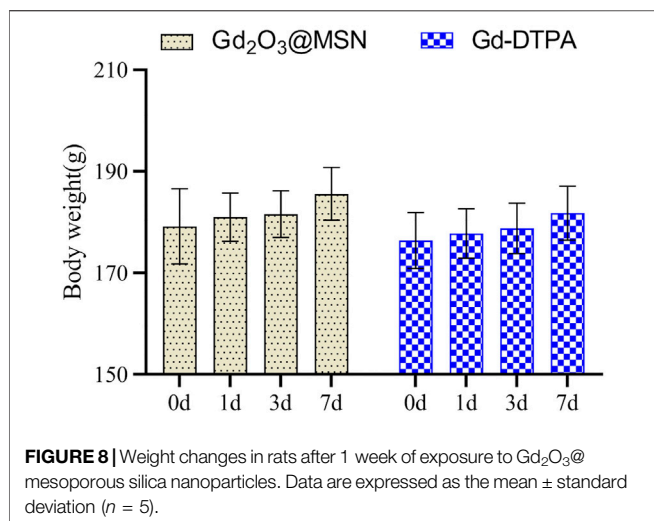


HAADF images (**Figure 3A**) and EDX elemental mapping images showed the significant and homogeneous signal of Gd in MSNs (**Figures 3B–E**), indicating the Gd^{3+} elements were evenly distributed across MSN structure.

Both surface area and pore distribution are critical for evaluating mesoporous materials; thus, all of the N_2 adsorption–desorption isotherms of $Gd_2O_3@MSN$ using BJH (**Figures 4A,B**) were evaluated. The samples exhibit typical type IV curves with an evident hysteresis loop, confirming its mesoporous nature (López et al., 2006; Liu et al., 2015; Philippart et al., 2017; Francesca et al., 2018; Naseem et al., 2020; Zhou et al., 2020). The BET test results also suggest that the surface area of the MSN was around $822.96\ m^2/g$, making them much larger than previous versions of similar compounds (Shao et al., 2011). The average pore size of these MSN was 3.49 nm and BJH revealed that they exhibited increased pore volume, $0.72\ cm^3g^{-1}$ compared to seminal MSN materials.

These structures were then validated using an FT-IR spectrometer. The FT-IR spectra for these NPs produced peaks at $801\ cm^{-1}$ and $455\ cm^{-1}$ corresponding to Si-OH





stretching, a peak at $1,080\text{ cm}^{-1}$ corresponding to Si-O-Si stretching vibration, and a peak at $3,433\text{ cm}^{-1}$ corresponding to the absorption bands of the hydroxyl group on MSN surface. These spectra also included a peak at $1,636\text{ cm}^{-1}$, corresponding to the bending vibration of -OH. Taken together, these patterns were representative of the characteristic absorption peaks of MSN materials (Figure 5) (Ni et al., 2016; He et al., 2019; Jiang et al., 2019; Cai et al., 2020).

3.2 T_1 Relaxivity and Gd Stability

The ability of pure Gd₂O₃@MSN was evaluated to enhance T_1 contrast using a 0.5 T NMI20 Analyst NMR system. The mean r_1 value (0.5 T) for Gd₂O₃@MSN was $51.85 \pm 1.38\text{ mM}^{-1}\text{ s}^{-1}$, which was much larger than that of Gd-DTPA ($4.62 \pm 0.43\text{ mM}^{-1}\text{ s}^{-1}$) (Figure 6A). The geometrical confinement of these structures resulted in an approximately 12-fold increase in the Gd₂O₃@MSN r_1 value when compared to that of the commercial Gd-DTPA, which suggested that these MSN could potentially be used as a T_1 contrast agent. The stronger contrast effect may be attributed to the tuneable pore structure which facilitates ready access of the water molecules (Parvesh et al., 2012), allowing for multiple water molecules to be coordinated with each Gd centre, decreasing Gd rotation within the framework (Lin et al., 2004; Jiang et al., 2019).

Figure 6B displayed the *in-vitro* T_1 -weighted images obtained using Gd₂O₃@MSN samples (numbered B1–B11) produced using different Gd concentrations, with these images clearly demonstrating that increasing Gd³⁺ concentration facilitates increased image brightness. Figure 5B describes similar *in-vitro* T_1 -weighted images using Gd-DTPA (numbered A1–A11) at the same concentrations (per Gd atom) as the Gd₂O₃@MSN images. This data clearly shows a significant increase in brightness in the Gd₂O₃@MSN images compared to the Gd-DTPA (Supplementary Table S1) images at the same concentration when captured at an MRI intensity of $1972.36 \pm 5.57\text{ a. u.}$ (Supplementary Table S2). Next, the signal-to-noise ratio (SNR) was calculated to evaluate the

contrast enhancement using finely tuned and broadly representative ROIs within the transverse images. The SNR for each image was then evaluated using the single image method described by the American Association of Physicists in Medicine (AAPM), using the following equation: $\text{SNR} = (S_{\text{central}} - S_{\text{background}}) / \text{SD}$ (AAPM Quality, 1990). These evaluations revealed that the SNR value of the Gd₂O₃@MSN images was much higher than that of Gd-DTPA images (Figure 6C).

Given the documented toxicity of free Gd³⁺ ions, its stability was evaluated within these MSN constructs as the first step for estimating its likely toxicity (Edyta et al., 2019; Lubinda et al., 2018). This was completed by placing Gd₂O₃@MSN (Gd³⁺, 100 mg/L) into PBS at different pH values (7.4, 5.5, and 4.5) and incubating these solutions for 48 h at 37°C, with both the pH and temperature designed to emulate various physiological conditions, including normal blood (pH 7.4), endosomes (pH 5.5) and lysosomes (pH 4.5) (Qi et al., 2019; Zhao et al., 2019). ICP-MS was then used to detect any free Gd ions in these solutions (Supplementary Figure S1). These evaluations revealed that there were very few free Gd³⁺ ions in any of these solutions (<1%) suggesting that Gd₂O₃@MSN was stable in these simulated *in-vitro* environments.

3.3 *In-Vitro* Cytotoxicity Studies

The cytotoxicity of Gd₂O₃@MSN was estimated using an *in-vitro* assay of AsPC-1, PaCa-2 and 4T1 cells (Figure 7). CCK-8 assay revealed that there was no significant cytotoxicity following 24 h of exposure to any of the NPs within the described concentration range, suggesting that these NPs exhibit little toxicity toward AsPC-1, PaCa-2 and 4T1 cells ($p > 0.05$).

3.4 *In-Vivo* Safety Evaluation

Healthy SD rats were treated with a high dose (100 mg/kg) of Gd₂O₃@MSN solution via intravenous (i.v.) injection and then monitored for up to 1 week to assess the *in-vivo* toxicity of Gd₂O₃@MSN. Negligible systemic toxicity or side effects were observed when using bodyweight measurement as a comparator (Figure 8) for any of these treatments with all the rats surviving the full-time course. Next, the main organs (heart, liver, spleen, lung, kidney) were harvested from these animals 7 days post-injection and were used to complete the histological assessment of these tissues using haematoxylin and eosin (H&E) staining. H&E evaluations revealed no clear changes in any of these tissues indicating acute (7 days) toxicity in response to Gd₂O₃@MSN exposure (Figure 9). A mini blood panel was also used to evaluate the potential cytotoxic effects of these NPs with all of the data suggesting the general health of these animals. (Table 2). These biochemical parameters included glutamic aspartate transaminase (AST), alanine aminotransferase (ALT), total bilirubin (T-BIL), blood urea nitrogen (BUN) and creatinine (Cr), all of which had no significant differences when compared with the control group (Gd-DTPA) on day 7 post-injection; thus, confirming that the primary function of both the kidneys and liver was not impaired post Gd₂O₃@MSN treatment. These results confirm the earlier findings around toxicity and support our hypothesis

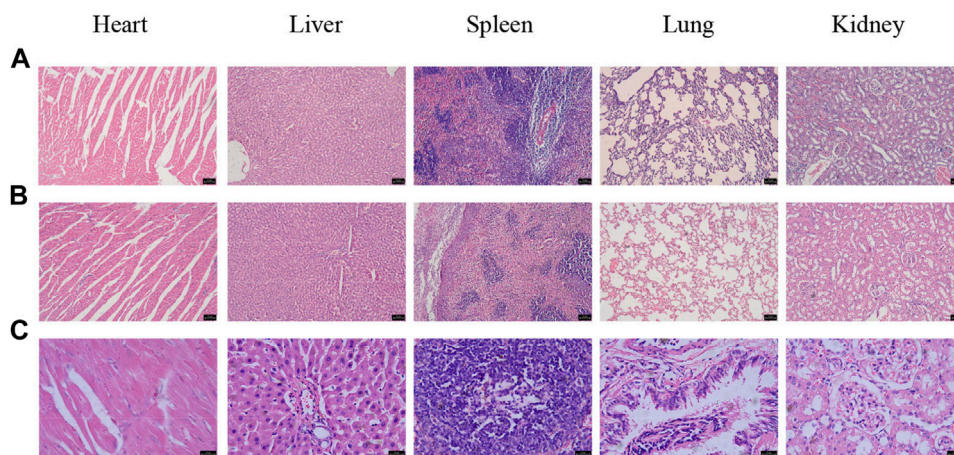


FIGURE 9 | Haematoxylin and eosin staining of the heart, liver, spleen, lung and kidneys from **(A)** Gd-gadolinium diethylene triamine pentaacetate treated Sprague-Dawley rats, scale bar: 75 μ m; **(B,C)** Gd₂O₃@MSN treated SD rats, scale bar: 75, 25 μ m (7 days post-injection).

TABLE 2 | Blood chemistry results for Sprague-Dawley rats injected with Gd₂O₃@mesoporous silica nanoparticles ($n = 5$).

	AST (U/L)	ALT (U/L)	T- BIL (μ mol/L)	BUN (mmol/L)	Cr (μ mol/L)
Gd ₂ O ₃ @MSN	151.08 \pm 22.88	125.61 \pm 17.46	0.68 \pm 0.13	8.86 \pm 1.65	31.32 \pm 4.17
Gd-DTPA	142.65 \pm 17.52	118.63 \pm 16.42	0.72 \pm 0.13	9.41 \pm 2.01	29.42 \pm 3.92

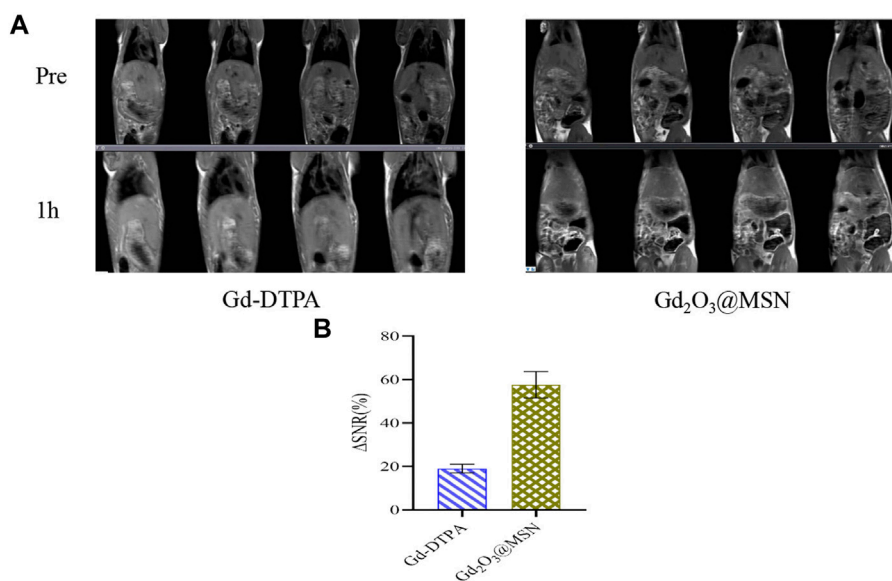


FIGURE 10 | **(A)** T_1 -weighted *in-vivo* magnetic resonance imaging of rats (coronal plane) collected before and 1 h after intravenous injection with Gd-gadolinium diethylene triamine pentaacetate (DTPA) or Gd₂O₃@mesoporous silica nanoparticles (MSN) (at a dose of 0.5 mg Gd per kg of body weight); **(B)** Signal-to-noise ratios 1 h after intravenous injection of Gd-DTPA or Gd₂O₃@MSN.

that this NP is well tolerated in living systems (Bong and Jaeyun, 2019; Yuan et al., 2020).

3.5 *In Vivo* Magnetic Resonance Imaging Studies

As-prepared contrast materials were injected into healthy SD rats for *in-vivo* imaging to evaluate Gd₂O₃@MSN as an *in-vivo* MRI contrast agent. Previous studies have shown that MSN adsorbs plasma proteins and interacts strongly with the tissue-resident macrophages in the mononuclear phagocyte system (MPS), leading to rapid blood clearance and accumulation in the liver and spleen (Gao et al., 2011; Ekkapongpisit et al., 2012; Li et al., 2016; Wang and Sun, 2020). Given this, we used the likely accumulation of our NPs in the hepatic Kupffer cells to determine our ROIs, focusing on the liver region. *T*₁-weighted images were collected before and 1 h after injection using a 3.0 T clinical MRI scanner. Our evaluations revealed that the liver region exhibited a significantly increased signal in animals treated with Gd-DTPA and Gd₂O₃@MSN (**Figure 10A**) when compared to the control. However, a comparison of the Gd-DTPA and Gd₂O₃@MSN images revealed a distinct increase in the liver signal from the novel contrast agent group, likely as a result of its higher *r*₁ value and increased accumulation in the liver due to its larger size. Next, the signal intensity (SI) was calculated to evaluate the contrast enhancement via the comprehensive evaluation of the ROIs in each of the transverse images (**Figure 10B**). The ΔSNR value for Gd₂O₃@MSN was (57.54 ± 6.10)%, which was much higher than that of Gd-DTPA (18.98 ± 1.96)%, confirming the significant improvement in MRI *T*₁ contrast when using Gd₂O₃@MSN for evaluating the liver.

4 CONCLUSION

To summarize, we successfully designed and fabricated a novel Gd₂O₃@MSN contrast reagent by one-step synthesis that produced a significant improvement in *T*₁ contrast capacity primarily mediated by the increased geometrical confinement effect of this product. The one-step synthesis method is easy and cost-effective, which would be beneficial for the development of novel MRI contrast agents and for expanding the potential use of high-performance contrast agents for MRI and diagnosis.

REFERENCES

- AAPM Quality (1990). Assurance Methods and Phantom for Magnetic Resonance Imaging[Z]. *AAPM Rep. No* 28, 287–295.
- Bong, G. C., and Jaeyun, K. (2019). Functional Mesoporous Silica Nanoparticles for Bio-Imaging Applications. *Interdiscip. Reviews-Nanomedicine. Nanobiotechnology*. 11, e1515. doi:10.1002/wnan.1515
- Cai, D. F., Han, C. Y., Liu, C., Ma, X. X., Qian, J. Y., Zhou, J. W., et al. (2020). Chitosan-capped Enzyme-Responsive Hollow Mesoporous Silica Nanoparticles for colon-specific Drug Delivery. *Nanoscale. Res. Lett.* 15, 123. doi:10.1186/s11671-020-03351-8
- Deng, Z. Y., Qian, Y. F., Yu, Y. Q., Liu, G. H., Hu, J. M., Zhang, J. Y., et al. (2016). Engineering Intracellular Delivery Nanocarriers and Nanoreactors from

DATA AVAILABILITY STATEMENT

The original contributions presented in the study are included in the article/**Supplementary Material**, further inquiries can be directed to the corresponding authors.

ETHICS STATEMENT

The animal study was reviewed and approved by Animal Ethics Committee of Qiqihar Medical University

AUTHOR CONTRIBUTIONS

Conceptualization and methodology, GL and LH, validation: ZL, JG, and MZ; investigation, ZL; resources:GL and LH; data curation, ZL; writing-original draft preparation, ZL; writing-review and editing, GL and LH; visualization, ZL; project administration and funding acquisition, GL. All authors have read and agreed to the published version of the manuscript.

FUNDINGS

This research was funded by Medical Sciences Project of Qiqihar Academy, grant number QMSI2019L-03, Basic scientific research business expenses of Heilongjiang Provincial Department of Education, grant number 2019-KYYWF-1251.

ACKNOWLEDGMENTS

We would like to thank the Qiqihar Medical Center Animal Center for helping with the model rats, the department of MRI at the first Affiliated Hospital of Qiqihar Medical University for MRI equipment support.

SUPPLEMENTARY MATERIAL

The Supplementary Material for this article can be found online at: <https://www.frontiersin.org/articles/10.3389/fchem.2022.837032/full#supplementary-material>

- Oxidation-Responsive Polymersomes via Synchronized Bilayer Cross-Linking and Permeabilizing inside Live Cells. *J. Am. Chem. Soc.* 138, 10452–10466. doi:10.1021/jacs.6b04115
- Edyta, W., Jakub, C., Agnieszka, K., Miroalaw, K., Leon, S., Artur, B., et al. (2019). Toxicity Mechanism of Low Doses of NaGdF₄: Yb³⁺, Er³⁺ Upconverting Nanoparticles in Activated Macrophage Cell Lines. *Biomolecules* 9, 14. doi:10.3390/biom9010014
- Ekkapongpisit, M., Giovia, A., Follo, C., Caputo, G., and Isidoro, C. (2012). Biocompatibility, Endocytosis, and Intracellular Trafficking of Mesoporous Silica and Polystyrene Nanoparticles in Ovarian Cancer Cells:effects of Size and Surface Charge Groups[J]. *Int. J. Nanomedicine*. 7, 4147–4158. doi:10.2147/IJN.S33803
- Francesca, E. C., Liliana, L., Lukas, G., Goldmann, W. H., and boccaccini, A. R. (2018). Synthesis and Characterization of Silver-Doped Mesoporous Bioactive

- Glass and its Applications in Conjunction with Electrospinning. *Materials (Basel)*. 11, 692. doi:10.3390/ma11050692
- Fraum, T. J., Ludwig, D. R., Bashir, M. R., and Fowler, K. J. (2017). Gadolinium-based Contrast Agents: A Comprehensive Risk Assessment. *J. Magn. Reson. Imaging* 46, 338–353. doi:10.1002/jmri.25625
- Gao, Y., Chen, Y., Ji, X. F., He, X. Y., Yin, Q., Zhang, Z. w., et al. (2011). Controlled Intracellular Release of Doxorubicin in Multidrug-Resistant Cancer Cells by Tuning the Shell-Pore Sizes of Mesoporous Silica Nanoparticles. *ACS Nano* 5, 9788–9798. doi:10.1021/nn20331010.1021/nn2033105
- He, K., Li, J. J., Shen, Y. X., and Yu, Y. Q. (2019). pH-Responsive Polyelectrolyte Coated Gadolinium Oxide-Doped Mesoporous Silica Nanoparticles (Gd₂O₃@MSNs) for Synergistic Drug Delivery and Magnetic Resonance Imaging Enhancement. *J. Mater. Chem. B*. 7, 6840–6854. doi:10.1039/c9tb01654f
- Hu, X. L., Liu, G., Li, Y., Wang, X. R., and Liu, S. Y. (2015). Cell-penetrating Hyperbranched Polyprodrug Amphiphiles for Synergistic Reductive Milieu-Triggered Drug Release and Enhanced Magnetic Resonance Signals. *J. Am. Chem. Soc.* 137, 362–368. doi:10.1021/ja5105848
- Jiang, w., Fang, H. Y., Liu, F. Q., Zhou, X., Zhao, H. Y., He, X. J., et al. (2019). PEG-coated and Gd-Loaded Fluorescent Silica Nanoparticles for Targeted Prostate Cancer Magnetic Resonance Imaging and Fluorescence Imaging. *Int. J. Nanomedicine*. 14, 5611–5622. doi:10.2147/IJN.S207098
- Koo, H., Huh, M. S., Ju, H. R., Lee, D. E., Sun, I. C., Choi, K., et al. (2011). Nanoprobes for Biomedical Imaging in Living Systems. *Nano. Today* 6, 204–220. doi:10.1016/j.nantod.2011.02.007
- Layek, B., Gidwani, B., Tiwari, S., Joshi, V., Jain, V., and Vyas, A. (2020). Recent Advances in Lipid-Based Nanodrug Delivery Systems in Cancer Therapy. *Cpd* 26, 3218–3233. doi:10.2174/1381612826666200622133407
- Li, X. W., Zhao, W. R., Liu, X. H., Chen, K. Q., Zhu, S. J., Shi, P., et al. (2016). Mesoporous Manganese Silicate Coated Silica Nanoparticles as Multi-Stimuli-Responsive T₁-MRI Contrast Agents and Drug Delivery Carriers. *Acta Biomater.* 30, 378–387. doi:10.1016/j.actbio.2015.11.036
- Li, Y. M., Yu, H. S., Qian, Y. F., Hu, J. M., and Liu, S. Y. (2014). Amphiphilic star Copolymer-Based Bimodal Fluorogenic/magnetic Resonance Probes for Concomitant Bacteria Detection and Inhibition. *Adv. Mater.* 26, 6734–6741. doi:10.1002/adma.201402797
- Lin, Y. S., Hung, Y., Su, J. K., Lee, R., Chang, C., Lin, M. L., et al. (2004). Gadolinium(III)-incorporated Nano-Sized Mesoporous Silica as Potential Magnetic Resonance Imaging Contrast Agents. *J. Phys. Chem.* 108, 15608–15611. doi:10.1021/jp047829a
- Liu, S. H., Pavlo, G., Wu, Z. S., Liu, Z. Y., Wei, W., Wagner, M., et al. (2015). Patterning Two-Dimensional Free-Standing Surfaces with Mesoporous Conducting Polymers. *Nat. Commun.* 6, 8817. doi:10.1038/ncomms9817
- López, N. A., Arcos, D., Izquierdo, B. I., Sakamoto, y., Terasaki, O., and Vallet, R. M. (2006). Ordered Mesoporous Bioactive Glasses for Bone Tissue Regeneration. *Chem. Mater.* 18, 3137–3144. doi:10.1021/cm060488o
- Lubinda, M., Steve, T. M., Rosa, B., Nicholas, G. D., Mara, C., and Santin, M. (2018). Gadolinium Tagged Osteoprotegerin-Mimicking Peptide: A Novel Magnetic Resonance Imaging Biospecific Contrast Agent for the Inhibition of Osteoclastogenesis and Osteoclast Activity. *Nanomaterials (Basel)*. 8, 399. doi:10.3390/nano8060399
- Mikada, M., Sukhbaatar, A., Miura, Y., Horie, S., Sakamoto, M., and Mori, S. (2017). Evaluation of the Enhanced Permeability and Retention Effect in the Early Stages of Lymph Node Metastasis. *Cancer Sci.* 108, 846–852. doi:10.1111/cas.13206
- Naseem, F., Zhi, Y., Farrukh, M. A., Hussain, F., and Yin, Z. Y. (2020). Mesoporous ZnAl₂Si₁₀O₂₄ Nanofertilizers Enable High Yield of Oryza Sativa L. *Sci. Rep.* 10, 10841. doi:10.1038/s41598-020-67611-4
- Ni, D., Bu, W., Ehlerding, E. B., Cai, W., and Shi, J. (2017). Engineering of Inorganic Nanoparticles as Magnetic Resonance Imaging Contrast Agents. *Chem. Soc. Rev.* 46, 7438–7468. doi:10.1039/c7cs00316a
- Ni, K., Zhao, Z. H., Zhang, Z. J., Zhou, Z. J., Yang, L., Wang, L. R., et al. (2016). Geometrically Confined Ultrasmall Gadolinium Oxide Nanoparticles Boost the T₁ Contrast Ability. *Nanoscale* 8, 3768–3674. doi:10.1039/c5nr08402d
- O'Connell, C. L., Nooney, R., and McDonagh, C. (2017). Cyanine5-doped Silica Nanoparticles as Ultra-bright Immunospesific Labels for Model Circulating Tumour Cells in Flow Cytometry and Microscopy. *Biosens. Bioelectron.* 91, 190–198. doi:10.1016/j.bios.2016.12.023
- Parvesh, S., Niclas, E. B., Glenn, A. W., Han-Byul, S., Zhou, G. Y., Nobutaka, I., et al. (2012). Gadolinium-Doped Silica Nanoparticles Encapsulating Indocyanine Green for Near Infrared and Magnetic Resonance Imaging. *Small* 8, 2856–2868. doi:10.1002/smll.201200258
- Philippart, A., Gómez, C. N., Arcos, D., Salinas, J., Boccardi, E., Vallet, R. M., et al. (2017). Novel Ion-Doped Mesoporous Glasses for Bone Tissue engineering: Study of Their Structural Characteristics Influenced by the Presence of Phosphorous Oxide. *J. Non. Cryst. Sol.* 455, 90–97. doi:10.1016/j.jnoncrysol.2016.10.031
- Phillips, M. A., Gran, M. L., and Peppas, N. A. (2010). Targeted Nanodelivery of Drugs and Diagnostics. *Nano. Today* 5, 143–159. doi:10.1016/j.nantod.2010.03.003
- Qi, Q. K., Chi, W. J., Li, Y. Y., Qian, Q. L., Chen, J., Miao, L., et al. (2019). A H-Bond Strategy to Develop Acid-Resistant Photoswitchable Rhodamine Spirolactams for Super-resolution Single-Molecule Localization Microscopy. *Chem. Sci.* 10, 4914–4922. doi:10.1039/c9sc01284b
- Shao, Y. Z., Liu, L. Z., Song, S. Q., Cao, R. H., Liu, H., Cui, C. Y., et al. (2011). A Novel One-step Synthesis of Gd³⁺-Incorporated Mesoporous SiO₂ Nanoparticles for Use as an Efficient MRI Contrast Agent. *Contrast. Media. Mol. Imaging* 6, 110–118. doi:10.1002/cmami.412
- Shen, Z., Wu, A., and Chen, X. (2017). Iron Oxide Nanoparticle Based Contrast Agents for Magnetic Resonance Imaging. *Mol. Pharmaceutics* 14, 1352–1364. doi:10.1021/acs.molpharmaceut.6b00839
- Shin, T.-H., Choi, Y., Kim, S., and Cheon, J. (2015). Recent Advances in Magnetic Nanoparticle-Based Multi-Modal Imaging. *Chem. Soc. Rev.* 44, 4501–4516. doi:10.1039/c4cs00345d
- Taylor, K. M., Kim, J. S., Rieter, W. J., An, H. Y., Lin, W. L., and Lin, W. B. (2008). Mesoporous Silica Nanospheres as Highly Efficient MRI Contrastagents. *J. Am. Chem. Soc.* 130, 2154–2155. doi:10.1021/ja710193c
- Vikas, G., Fernando, C., Frank, G. S., Emanuel, K., and Scott, B. R. (2017). Gadolinium Deposition in the Brain:summary of Evidence and Recommendations. *Lancet Neurol.* 16, 564–570. doi:10.1016/S1474-4422(17)30158-8
- Wang, L. Q., and Sun, X. F. (2020). Mesoporous Silica Hybridized with Gadolinium(III) Nanoplatfor for Targeted Magnetic Imaging - Guided Photothermal Breast Cancer Therapy. *Dose Response* 18, 1559325820902314. doi:10.1177/1559325820902314
- Xia, N., Deng, D. H., Mu, X. S., Liu, A., Xie, J. X., Zhou, D. D., et al. (2019). Colorimetric Immunoassays Based on Pyrroloquinoline Quinone-Catalyzed Generation of Fe(II)-ferrozine with Tris(2-Carboxyethyl)phosphine as the Reducing Reagent. *Sensors Actuators B: Chem.* 306, 127571. doi:10.1016/j.snb.2019.127571
- Yuan, D. H., Connor, M. E., and Jason, J. D. (2020). Mesoporous Silica Nanoparticles in Bioimaging. *Materials (Basel)* 13, 3795. doi:10.3390/ma13173795
- Zhao, J. W., Yang, H., Li, J. L., Wang, Y. J., and Wang, X. (2019). Fabrication of pH-Responsive PLGA(UCNPs/DOX) Nanocapsules with Upconversion Luminescence for Drug Delivery. *Sci. Rep.* 7, 18014. doi:10.1038/s41598-017-16948-4
- Zhou, Z. Y., Li, X., Guo, D., Shinde, D. B., Lu, D. W., Chen, L., et al. (2020). Electropolymerization of Robust Conjugated Microporous Polymer Membranes for Rapid Solvent Transport and Narrow Molecular Sieving. *Nat. Commun.* 11, 5323. doi:10.1038/s41467-020-19182-1

Conflict of Interest: The authors declare that the research was conducted in the absence of any commercial or financial relationships that could be construed as a potential conflict of interest.

Publisher's Note: All claims expressed in this article are solely those of the authors and do not necessarily represent those of their affiliated organizations, or those of the publisher, the editors and the reviewers. Any product that may be evaluated in this article, or claim that may be made by its manufacturer, is not guaranteed or endorsed by the publisher.

Copyright © 2022 Li, Guo, Zhang, Li and Hao. This is an open-access article distributed under the terms of the Creative Commons Attribution License (CC BY). The use, distribution or reproduction in other forums is permitted, provided the original author(s) and the copyright owner(s) are credited and that the original publication in this journal is cited, in accordance with accepted academic practice. No use, distribution or reproduction is permitted which does not comply with these terms.